SMALL IMPACT CRATERS IN THE LUNAR REGOLITH – THEIR MORPHOLOGIES, RELATIVE AGES, AND RATES OF FORMATION

H. J. MOORE[1], J. M. BOYCE[2] and D. A. HAHN[3]

[1] *U.S. Geological Survey, Menlo Park, California, U.S.A.*

[2] *NASA Headquarters, Washington, D.C., U.S.A.*

[3] *U.S. Geological Survey, Flagstaff, Arizona, U.S.A.*

(Received December 21, 1979)

Abstract. Apparently, there are two types of size-frequency distributions of small lunar craters (≃ 1–100 m across): (1) crater production distributions for which the cumulative frequency of craters is an inverse function of diameter to power near 2.8, and (2) steady-state distributions for which the cumulative frequency of craters is inversely proportional to the square of their diameters. According to theory, cumulative frequencies of craters in each morphologic category within the steady-state should also be an inverse function of the square of their diameters. Some data on frequency distribution of craters by morphologic types are approximately consistent with theory, whereas other data are inconsistent with theory.

A flux of crater producing objects can be inferred from size-frequency distributions of small craters on the flanks and ejecta of craters of known age. Crater frequency distributions and data on the craters Tycho, North Ray, Cone, and South Ray, when compared with the flux of objects measured by the Apollo Passive Seismometer, suggest that the flux of objects has been relatively constant over the last 100 m.y. (within 1/3 to 3 times of the flux estimated for Tycho).

Steady-state frequency distributions for craters in several morphologic categories formed the basis for estimating the relative ages of craters and surfaces in a system used during the Apollo landing site mapping program of the U.S. Geological Survey. The relative ages in this system are converted to model absolute ages that have a rather broad range of values. The range of values of the absolute ages are between about 1/3 to 3 times the assigned model absolute age.

1. Introduction

Objects from space have been striking the lunar surface and producing impact craters for billions of years. The sizes of the craters produced by the objects range from tiny craters a tenth of a micrometer (μm) across on lunar rocks (Morrison *et al.*, 1973) to gigantic basins hundreds of kilometers (km) across (Gilbert, 1893). Average rates of formation of impact craters larger than 250 m have clearly decreased since 4 g.y. ago (Soderblom and Lebofsky, 1972). In recent times, since 1 g.y. ago, changes in rates of formation of impact craters may have been small. The rate of formation of craters can be addressed by considering six categories: (1) microcraters 0.1 μm to several millimeters across, (2) very small craters several millimeters to about 1 m across, (3) small craters about 1 m to about 100 m across, (4) intermediate size craters from about 100 m across to 1 km across, (5) large craters a few kilometers to as much as 100 km across, and (6) basins hundreds of kilometers across. In general, the larger the craters, the farther backward in time their history can be traced. Microcratering rates can be traced about 20 m.y., and the rate of microcrater formation appears to have been fairly constant during the last 20 m.y.

The Moon and the Planets **23** (1980) 231–252. 0165–0807/80/0232–0231$03.30.

(Morrison *et al.*, 1973); rates of formation of intermediate-size craters can be traced backward to about 3.3 g.y. ago, and the rate appears to have been constant (Guinnes and Arvidson, 1977); rates of formation of very small and large craters are still a problem; and rates of formation of lunar basins decreased from large values some 4.0 to 4.3 g.y. ago to zero about 3.85 g.y. ago. This paper is concerned, chiefly, with the flux producing small craters (1 m to about 100 m across) during the last billion years.

A system of estimating relative ages of craters (Trask, 1971) is calibrated using crater frequency distributions on the flanks of craters with known absolute ages and data on present-day meteoroid fluxes so that rough estimates of absolute ages can be made for some small- to intermediate-size craters. Calibration of the relative ages requires a discussion of (1) crater frequency distributions of small craters, (2) the concepts and characteristics of steady-state surfaces, (3) the system of estimating relative ages, and (4) the method used to assign absolute ages to the relative ages. These four subjects are discussed below and followed by a discussion of present-day and past impact rates or fluxes.

2. Crater Frequency Distributions

There are four fundamental concepts required to understand the frequency distributions of small lunar craters: (1) craters are continuously produced by impacts on the lunar surface with a size frequency distribution extending from very small craters to very large craters, and the relative frequency of the smaller craters is much greater than the larger ones, (2) craters are eroded and destroyed by subsequent impacts, the chief effect being erosion of larger craters by impacts producing smaller craters, (3) lunar surfaces attain a steady-state condition in which craters below a limiting size are destroyed as rapidly as they are produced, and (4) craters degrade in a regular manner with time so that each morphologic type of crater is in a steady state.

2.1. Crater Production Curves

Craters are formed continuously by impacts with the lunar surface. This fact has been established by studies of Apollo data and returned samples (Morrison *et al.*, 1973); Duennebier *et al.*, 1975) as well as by previous studies (see, for example, Shoemaker, 1965). Lunar crater frequency distributions that directly reflect the crater production curves of small lunar craters are of the form

$$N = KD^{\alpha}, \tag{1}$$

where N is the cumulative number of craters per unit area with diameters equal to or larger than D, K is the net accumulated flux or the cumulative frequency corresponding to the intersection of the crater production curve with an ordinate corresponding to a given crater diameter; K increases with age of a surface, and α is the population index and has a value near -2.8 for the range of sizes of craters considered here.

At the Surveyor landing sites, α is near -3 for craters 10 m to 1 km across (Shoemaker *et al.*, 1969). A polynominal equation describing lunar crater frequency distributions over

the range of 300 m to 2.0 km (Neukum *et al.*, 1975) is compatible with an exponent or population index near -3 craters from about 300 m to about 500 m, but for craters 500 m to about 2 km the exponent or population index is near -3.4. As will be shown later, our data on craters from 4 to 50 m across indicate that α is near $(-)$ 2.8. The craters are produced by objects from space (primary craters) and ejecta from lunar craters (secondary craters). Relative importance of the two kinds of craters is a matter of debate. Some authors believe that small craters are chiefly primary (Moore, 1964; Gault, 1970) whereas others believe that small craters are chiefly secondary (Shoemaker, 1965; Soderblom. 1970). It appears probable that the small craters considered here are chiefly primary craters because our data on North Ray and Cone craters, the data of Shoemaker (1965) for Tycho, and the data of Guinness and Arvidson (1977) for Tycho and Copernicus floor have population indices (α) that are nearly the same ($\simeq -2.8$). Locally, secondary impact craters dominate, such as along the rays of fresh impact craters and around the periphery of ejecta of fresh craters, but 'average' surfaces have craters that are chiefly primary. Idealized crater frequency distributions of small craters for three ages of surfaces are shown in Figure 1.

Because average lunar surfaces are continually bombarded by objects producing small craters, young surfaces have fewer craters than older ones. The net accumulated fluxes for three surfaces (K_1, K_2, K_3, in Figure 1) increase with their relative ages. Crater frequency distributions with the form of Equation (1) are found only for the larger sizes of small craters because theoretical considerations show that the area occupied by the smaller sizes of small craters produced by primary impacts exceeds the area of the surface on which they are produced within a short time (Moore, 1964; Shoemaker, 1965; Marcus, 1970; Soderblom, 1970). Thus, subsequent impacts must destroy previously formed craters. Erosion of larger craters by smaller ones may be the chief mechanism of crater destruction (Soderblom, 1970), but infilling by deposition of ejecta is also important (Moore, 1964; Marcus, 1970; Soderblom. 1970). Erosion and infilling destroy small craters as rapidly as they are produced so that the surface reaches a steady state (below a limiting size, called D_{CS}) in which the general appearance of the cratered surface remains the same although the details are continually changing.

2.2. STEADY-STATE-CURVES

Steady-state size-frequency distributions of craters on lunar surfaces are well established by observation (Trask, 1966; Shoemaker *et al.*, 1969), experimentally demonstrated (Gault, 1970; Moore *et al.*, 1974), and theoretically demonstrated (Moore, 1964; Marcus, 1970; Soderblom, 1970). In general, the steady-state distribution for lunar plains can be represented by an equation of the form

$$M = CD^{-2}, \tag{2}$$

where M is the cumulative frequency of craters per unit area with diameters equal to and greater than D, C is a parameter that varies with the manner in which craters are destroyed and the physical properties of the surface (Moore, 1964; Marcus, 1970. Soderblom, 1970;

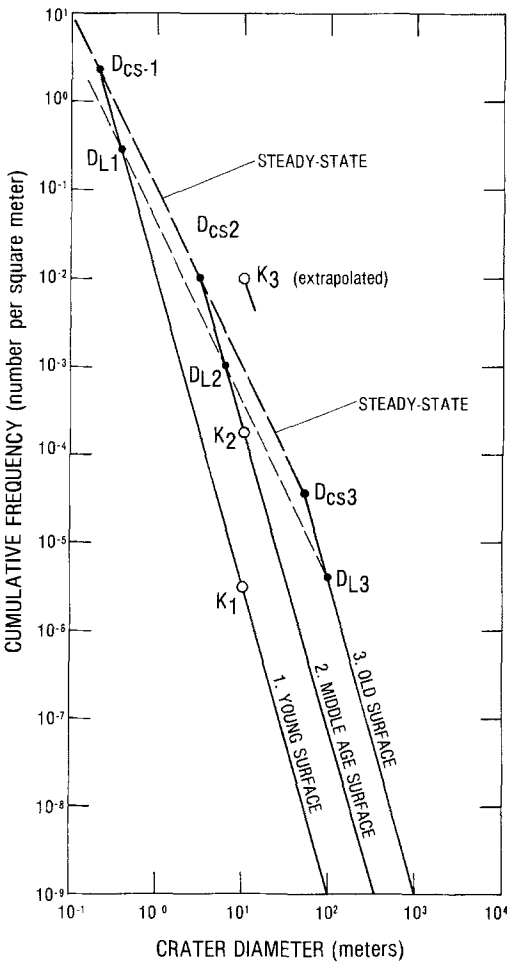

Fig. 1. Diagrammatic cumulative size–frequency distributions of craters for three ages of surfaces. Distribution for each surface is composed of two parts: a crater production distribution (solid line) and a steady-state distribution (long dashed line). Crater production distribution of young surface joins steady-state distribution at D_{CS_1}; largest crater eroded to an interior slope angle of 1° is D_{L_1}; net accumulated flux (K in Equation (1)) is K_1. Crater production distribution of middle age surface joins steady-state distribution at D_{CS_2}; largest crater eroded to an interior slope angle of 1° is D_{L_2}; net accumulated flux is K_2. Crater production distribution of old surface joins steady-state distribution at D_{CS_3}; largest crater eroded to an interior slope angle of 1° is D_{L_3}; net accumulated flux is K_3. Short dashed line connects values of D_L for the three surfaces and is parallel to the steady-state distribution. Note diameters corresponding to D_{CS_1}, D_{CS_2}, and D_{CS_3} increase with age of surface; diameters of D_{L_1}, D_{L_2}, D_{L_3} also increase with age of surface; and, cumulative frequencies corresponding to K_1, K_2, and K_3 increase with age of surface. In practice, the crater production distribution and steady-state distribution join in a gradual way so that D_{CS} is a point obtained by mathematical or graphical methods.

Morrison *et al.*, 1973); the value of the parameter C is 0.0794 craters for lunar plains (Moore, 1964; Trask, 1966; Shoemaker *et al.*, 1969).

Although the exponent on D is (−) 2 for most lunar surfaces, other values are possible where crater destruction is the result of thermal creep on steep slopes of rugged terrain, seismic erosion, and blanketing (see, for example, Moore, 1964; Marcus, 1970), and the form of the crater production frequency distribution may alter this exponent (Moore *et al.*, 1974).

Equations (1) and (2) join at a pont with the same frequency and diameter (Figure 1). The upper limiting crater diameter at which this join occurs is D_{CS} (Shoemaker *et al.*, 1969). It should be realized that this join is a mathematical construction and that in reality the crater production curve joins the steady state curve in a gradual manner. Solving Equations (1) and (2) for D_{CS} shows that D_{CS} is a linear function of K only when $\alpha = -3$; i.e.,

$$D_{CS} = \frac{C}{K}\frac{1}{2+\alpha} \tag{3}$$

D_L (Figure 1) is related to K by an equation with the same form as Equation (3) when C is replaced by an appropriate constant. This relation has been experimentally demonstrated for craters several 100 m to several km across. For craters larger than 300 m to 2.0 km, $\alpha \simeq -3.4$ (Neukum, 1977) so that D_L should be directly proportional to $K^{0.7}$ by Equation (3). This is in reasonable agreement with the experimentally derived relationship for intermediate size craters which $D \propto K^{0.6}$ (Neukum, 1977).

2.3. Curves for Morphologic Types

Cumulative frequencies of craters with given morphologies or states of preservation should have approximately the same mathematical form as the steady state, but the curves should lie below the steady state curve and intersect the crater production curve at larger diameters. This theoretical relation is shown in Figure 2 using one model (Moore, 1964, 1971) and is predicted by other models (Soderblom, 1970; Soderblom and Lebofsky, 1972). According to theory, then, the fraction of craters (relative frequency) with the same morphologies and equal diameters should be the same at any diameter smaller than D_{CS} (Table I), and their cumulative numbers should increase as the inverse square of their diameters. In Figure 2, craters are grouped into four morphologic types: (1) fresh craters retain 31/32 or more of their original relief, (2) young craters retain 31/32 to 3/4 of their original relief, (3) mature craters retain 3/4 to 1/2 of their original relief, and (4) old craters retain 1/2 to none of their original relief. Cumulative frequencies of fresh craters are represented by the line with a (−) 2 slope between the words fresh and young in Figure 2. The line between young and mature represents the cumulative frequency of fresh and young craters, and so forth. The uppermost line represents the cumulative frequency of all craters.

Observational evidence for steady-state frequency distributions for individual morphologic types was first reported for small craters photographed by Rangers 7 and 8 for which the size-frequency distribution of eumorphic or fresh craters were found to be well

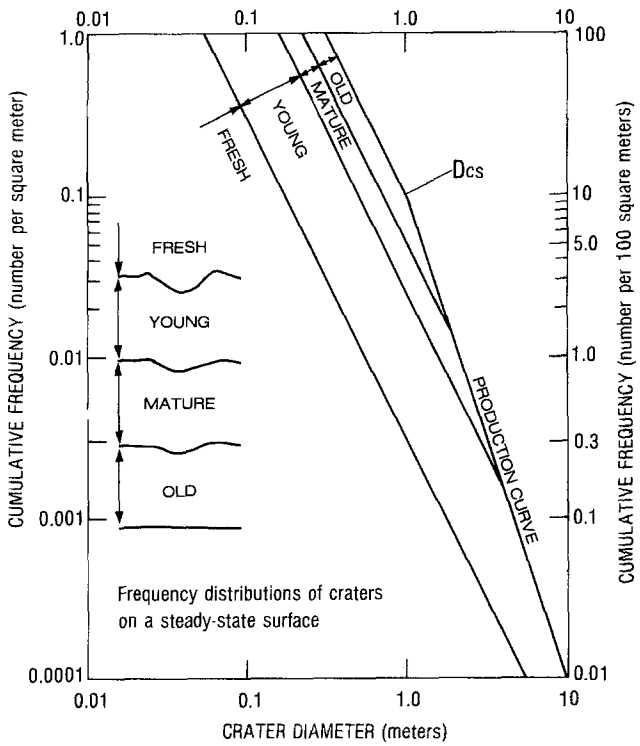

Figure 2. Graph showing cumulative size–frequency distributions of craters of various morphologies and sizes for a steady-state surface. Crater production curve and upper line represent cumulative frequencies of fresh, young, mature, and old craters, i.e., all craters. Part of crater production curve and second line represents cumulative frequencies of fresh, young, and mature craters. Part of crater production curve and third line represents cumulative frequencies of fresh and young craters. Lowermost line represents cumulative frequencies of fresh craters. Lowermost curve joins crater production at a point off the graph to the lower right. Crater profiles define boundaries between various morphologies (after Moore, 1971).

below the steady-state curve and approximately parallel to it (Trask, 1966, Figure 4, p. 257).

A number of preliminary crater counts made on Lunar Orbiter photographs for Apollo site selection purposes show the same pattern (Figure 3a, curve 1) such as those for site III P 12 and others (Langley Research Center, 1967b, Figure 18, 22, and 37). Counts of 'eumorphic' craters by three observers also yield cumulative size–frequency distributions that are essentially parallel to the steady-state curve (Figure 3a). Although the observers do not have the same definition of 'eumorphic', they do agree on the general form of the curves. All of the information for these counts, which were partly furnished by N. J. Trask (written communication, 1978), cannot be recovered but that which can is tabulated in the Appendix and general locations can be found in Langley Research Center (1967a, b). A least-squares fit to the crater size–frequency distribution of eumorphic craters in Sinus Medii (Figure 3a, curve 2, counted by N. J. Trask) yields a slope of (—) 2.07 ± 0.05 (± 1σ).

TABLE I

Characteristics and relative frequencies of morphologic types of craters in the ideal steady-state

Morphological type	Fraction of original relief	Relative frequency or fraction of craters	Cumulative relative frequency or fraction of craters
Old craters	> 0–1/2	1/2	1
Mature, young, and fresh	1/2–3/4	1/4	1/2
Young and fresh	3/4–1	1/4	1/4
Fresh craters	31/32–1	1/32	1/32

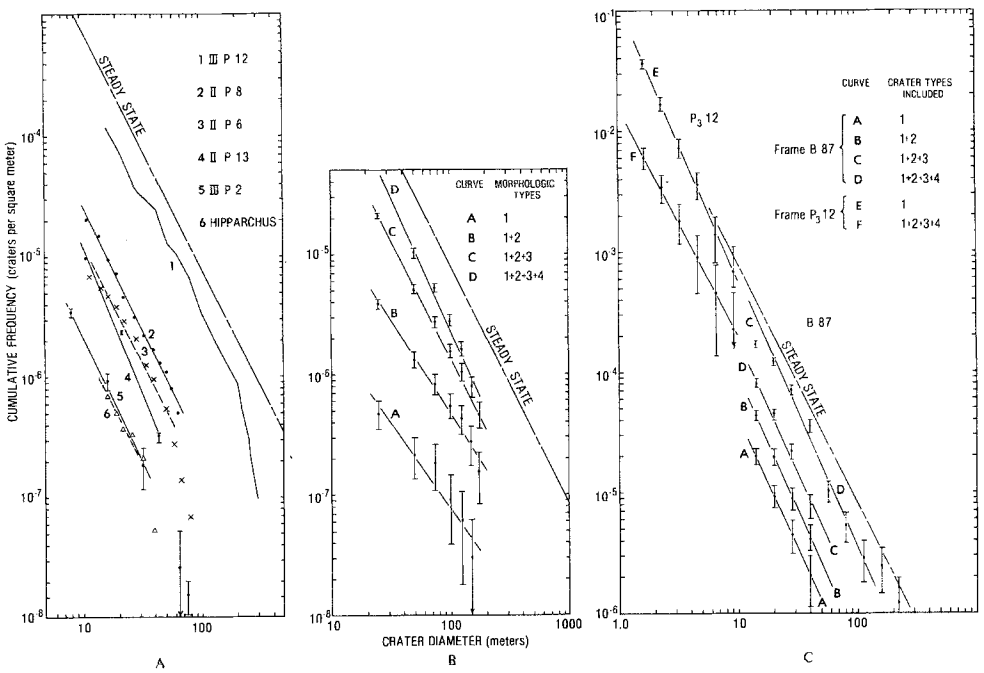

Figure 3. Observed cumulative size–frequency distributions of (a) eumorphic craters obtained by various independent observers, (b) four morphologic types of craters obtained using Lunar Orbiter III high-resolution frame H199, and (c) four morphologic types of craters obtained using high-resolution Ranger 9 pictures. Note in (a) that slopes of curves for eumorphic craters are near (—) 2 and flatter than the crater production curve; vertical displacements of curves caused by the different definitions of 'eumorphic' used by the various observers. Position of curve 1 probably controlled by sun elevation angle of pictures used. Solid straight lines are least-squares fits to data; dashed straight lines have slope of (—) 2. Morphologic types of craters included in curves of (b) are described in text; curve A includes type 1 Craters; curve B includes types 1 and 2; curve C includes types 1, 2 and 3; and curve D includes types 1, 2, 3 and 4; solid straight lines are least-squares fits to data. Note that curves C and D agree well with theory but that A and B do not. Morphologic types of craters included in curves of (c) are discribed in text; curve A includes type 1 craters; curve B includes types 1 and 2; curve C includes types 1, 2, and 3; curve D includes types 1, 2, 3, and 4; curve E includes types 1, 2, 3, and 4; curve F includes type 1 craters. Error bars in (b) and (c) calculated using standard procedures (National Aeronautic and Space Administration, 1978) and data appear in Appendix (as per National Aeronautic and Space Administration, 1978).

Such a slope is acceptably close to the (—) 2 of the theoretical value. A least-square fit to the crater size–frequency distribution of eumorphic craters in western Mare Fecunditatis (Figure 3a, curve 5, counted by H. J. Moore) has a slope of (—) 2.11 ± 0.12 (± 1σ), which is again close to the expectations of theory. Numbers for counts in southwestern Mare Tranquillitatis and Hipparchus (Figure 3a, curves 3 and 6, counted by S. Wilson) are not available, but the distributions are reasonably close to the dashed lines, which have slopes close to (—) 2. The slopes of the cumulative distribution of craters (curve 4 in Figure 3a) used by Quaide and Oberbeck (1968) in their regolith thickness studies is near (—) 2.46 (fit to diameters from 10.75 to 42.55 m) and (—) 2.3 (fit to diameters from 10.75 to 37.25 m).

We have attempted a more precise measurement of the relative frequencies of crater types to classify craters in Oceanus Procellarum, a relatively blocky mare area, by size into four morphological types (see Appendix for data): (1) those with well-developed rays, secondary craters observable on high-resolution photographs, abundant blocks, and radial structures on rim deposits, (2) those with no distinct rays, but with bright rim deposits, abundant blocks on rims, and moderately subdued rim crests, (3) strongly subdued craters with few blocks on rims, and (4) shallow bowl-shaped craters with rare blocks. The results, shown in Figure 3b, indicate that over-all slopes are distinctly less than the (—) 2.8 of the crater production curve. For curves C and D, with large numbers of craters, the slopes of the curves are (—) 2.26 and (—) 2.00, respectively, for craters 175 m and less (Figure 2b). Results for type 1 (curve A) and types 1 + 2 (curve B) do not conform to theory (slopes are (—) 1.53 and (—) 1.52, respectively). This difference is puzzling in view of the fact that other data (Figure 3a) conform with theory so well over comparable sizes and frequency ranges. Curve 2 (Figure 3a), which also applies to a blocky mare area, has a steeper slope ((—) 2.45) over a similar range of sizes. The departure from theory in our observations may be the result of a too rigorous application of the criterion of blocks in the rims of the smaller craters for an area where there are two layers: the regolith and a hard substrate. This results in an underestimate of the numbers of type 1 and type 2 craters at the smaller sizes where the craters are formed in the regolith and do not interact with the substrate of rocks.

Some data are in conflict with results reported above. In particular, relative frequencie s of morphologic types of craters shown in Ranger pictures were found to vary with diameter in an unsystematic way (Trask, 1967; Chapman, 1968). Because of this, we classified craters shown in Ranger 9 photographs B-87 and P3 12 (National Aeronautics and Space Administration, 1966) into four categories (1) craters with rims and shadow extending more than half way across the crater, (2) craters with subdued rims and shadows extending half to one-quarter way across the crater, (3) craters with little or no rims and shadows extending less than one-quarter way across the crater, and (4) shadowless depressions. The results are mixed (Figure 3c and Appendix). Least-squares fits for the larger craters shown on B-87 yield results as compatible with theory as those from counts of Lunar Orbiter pictures (Figures 3a and b). Slopes for the least-squares fits (Figure 3c) are (—) 2.18 (curve A), (—) 2.26 (curve B), (—) 2.21 (curve C), and (—) 2.29 (curve D) for all

craters in categories 1, 1 + 2, 1 + 2 + 3, and all craters, respectively. For the counts on photograph P3 12, the frequency distribution for all craters (Figure 3c, curve E) was fairly compatible with that obtained from photograph B-87, but the category 1 craters were about a factor of five larger than the number expected from counts on photograph B-87 (Figure 3c, curve F). Despite this difference, the slope of the type 1 craters ((−) 1.92) was near the expected value ((−) 2). Frequency distributions for category 1 + 2 and 1 + 2 + 3 groupings had slopes less than ((−) 2) and do not fit the scheme. The reasons for the differences appear to be the result of local differences in crater densities, perhaps due to secondary impacts, because some areas in the Ranger 9 photographs appear smoother and less cratered than others.

Measured ratios of the number of unshadowed and shadowed craters plotted against crater diameter show that the size–frequency distributions of morphologic types are parallel to the steadystate curve below a critical diameter (Soderblom and Lebofsky, 1972). Both the ratio and the critical diameter depend on the sun elevation angle. Above the critical diameter, the ratio is an inverse function of crater diameter and becomes zero at the largest diameters when sun elevation angles are not too large or too small. Below the critical diameter, the ratio is constant. This evidence lends considerable justification for postulating the existence of steady-state size–frequency distributions for craters of each morphologic type.

On the basis of the evidence cited above, but with considerable reservations, we accept the postulate that *each* morphologic category of small craters has a steady-state distribution. Evidence for validity of this postulate is better founded for craters about 10 m across to several 100 m across; for those in millimeter- to 10-m size range the evidence is weak, but evidence for a steady-state distribution of all craters is better founded. In subsequent discussions, the postulate that steady-state distributions of each morphologic type, as described by Trask (1971) and outlined below, is extrapolated to millimeter-size craters. However, the arguments depend chiefly on a steady-state distribution for all craters and this appears to us to be reasonably well founded.

3. Relative Ages of Craters

As part of Apollo site mapping, a relation between relative ages of craters, their morphologies, and their diameters was postulated (Trask, 1971) and represented in a diagram (Figure 4). In the representation (Figure 4), horizontal lines are isochrons and correspond to the crater production curves (see Figures 1 and 2) so that the ordinate is relative age with a logarithmic scale. The abscissa represents crater size. Oblique lines correspond to empirical steady-state curves for seven morphologic classes of craters:

(a) very fresh craters with well developed rays, secondary craters observable on high-resolution photographs, radial structures on rim deposits;

(b) well-developed rays, abundant blocks on rims;

(c) no distinct rays, rim deposits appear bright, abundant blocks on rim but fewer than above, rim crest slightly subdued;

(d) no rays, rim crests, moderately subdued, some blocks on rims of craters in mare;

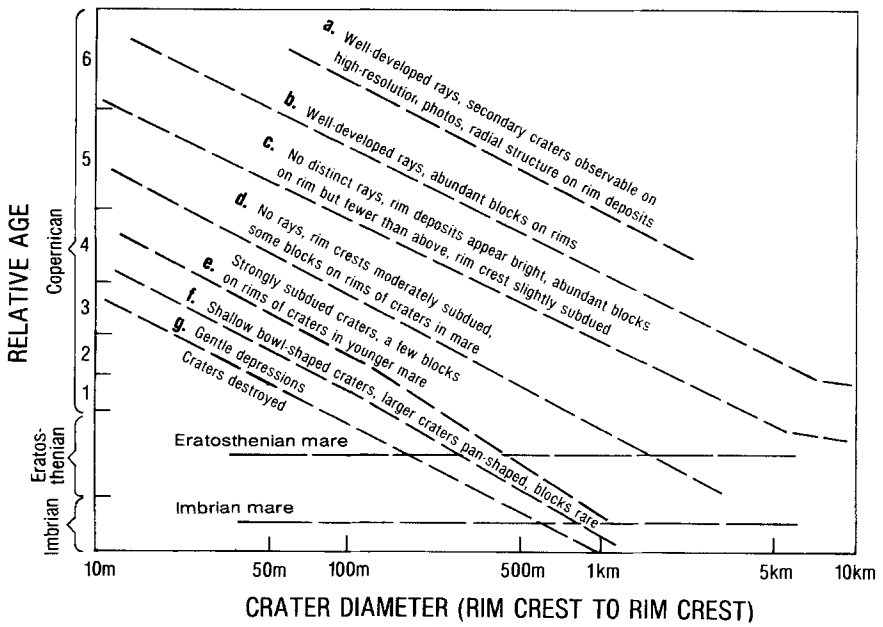

Figure 4. Assumed relations among sizes, crater morphologies, and relative ages of craters from 10 m to 10 km in diameter followed in large-scale geologic mapping of Apollo landing sites. Categories are intergradational and examples are shown in Figure 2 of Trask (1971). Horizontal lines are isochrons indicating crater populations on relatively young and relatively old mare materials (from Trask, 1971). Letters assigned to morphologic categories correspond to those used later in Figure 7.

(e) strongly subdued craters, a few blocks on rims of craters in younger mare;

(f) shallow bowl-shaped craters, larger craters pan-shaped, blocks rare;

(g) gentle depressions.

The line in the diagram separating gentle depressions and craters destroyed represents the upper limit of the steady-state. Numbers corresponding to isochron intervals were assigned for relative ages of craters in the Copernican System.

Diameters corresponding to intersections of horizontal lines with the boundary between gentle depressions and craters destroyed may be interpreted as D_{CS} or D_L depending on the location of the boundary on the diagram (compare Figure 4 and Figures 1 and 2). In a general way, the diagram of Figure 4 can be thought of as the plot in Figure 2 rotated 70° clockwise in the plane of the paper and then 180° about an isochron (which corresponds to a crater production curve).

In Apollo site mapping, Figure 4 was chiefly used to obtain the relative ages of individual craters and to estimate roughly the relative ages of geologic map units by visual inspection of the larger craters of the various morphologies near the point where their individual steady-state curves join the crater production curve. For example, surfaces with shallow bowl-shaped craters near 300–500 m across and smaller would be Eratosthenian, whereas surfaces with shallow bowl-shaped craters near 30–50 m across and smaller would be Copernican (C-2 to C-3 in Figure 4).

Absolute ages can be correlated with the relative ages of Figure 4 in two ways:

(1) locating surfaces with known absolute ages using analyses of their superposed crater frequency distributions, and

(2) locating individual craters with known absolute ages, diameters, and the value of D_{CS} derived from crater frequency distributions on their ejecta. This second approach is discussed in the following section.

4. Calibration of Figure 4

In a pioneering effort, Swann and Reed (1974) correlated craters of known absolute ages and diameters with the Copernican relative age numbers (Figure 4) established by visual inspections of other workers. Here, we have (1) counted small craters on the near flanks of larger craters with known absolute ages; (2) established the cumulative frequency of craters with diameters of 10 m and larger (N_{10}) and used this frequency to calculate K in Equation (1) with $\alpha = (-)\,2.8$; (3) calculated the value of D_{CS} using Equation (3) with $\alpha = (-)\,2.8$ and with $C = 0.0794$; (4) plotted the values of D_{CS} as a function of absolute age of the crater; (5) constructed a model relation with D_{CS} and absolute age; and (6) then located the isochrons on the basis of the model. The craters are located on Figure 4 according to the calculated values of D_{CS} and their diameters. Because the crater frequency distributions and diameters are data derived independently of absolute ages, the plotted points scatter and, therefore, model ages differ somewhat from their actual ages.

The craters employed in the calibration of Figure 4 are Tycho, North Ray, Cone, and South Ray. Although crater counts for Copernicus were not obtained, and estimate of D_{CS} from the known D_L value was obtained so that it could be included (Table I). Crater counts for North Ray, Cone, and South Ray were obtained from the best available photography, and the results and experimental conditions are tabulated in the Appendix. On the basis of least-squares fits to the data, exponent or population indices for the distributions (α) were $(-)\,2.81 \pm 0.12$ ($\pm 1\sigma$) and $(-)\,2.75 \pm 0.13$ ($\pm 1\sigma$) for North Ray and Cone (Figure 5). These values compare well with the (—) 2.93 obtained from counts of craters near Surveyor VII (Shoemaker *et al.*, 1969) and the (—) 2.7 for Tycho craters (Guinness and Arvidson, 1977). These population indices form the basis for our selection of an index of (—) 2.8. Exceptionally few craters were found at South Ray, and an unreliable value of (—) 4.87 was obtained for α (Figure 5). Cumulative numbers of craters with diameters of 10 m and larger (N_{10}) were calculated for the craters (Table II, Figure 5), and then new values for the net accumulated fluxes (K_a) were calculated using N_{10} and assuming that α was (—) 2.8, exactly (Table II). Using the recalculated net accumulated fluxes (K_a), an exponent (α) equal to (—) 2.8, and a value of C of 0.0794 in Equation (2), the limiting size was calculated with Equation (3). The results of these calculations of K_a and D_{CS} indicate that the relative ages of the craters, from oldest to youngest, are Tycho, North Ray, Cone Crater, and South Ray. The estimated D_{CS} for Copernicus indicates it is substantially older than Tycho (Table II).

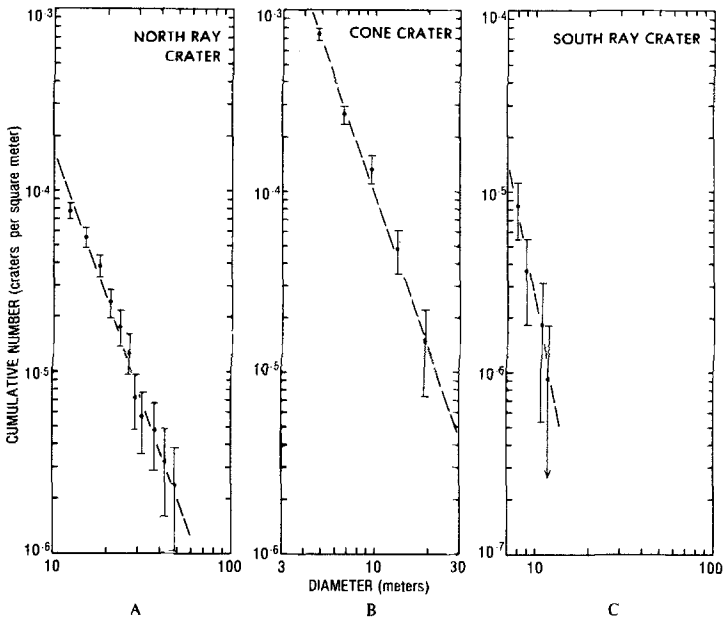

Figure 5. Cumulative size-frequency distributions and fractions of area covered by craters for (a) North Ray, (b) Cone, and (c) South Ray craters. Straight dashed lines are least-squares fits to data.

Absolute ages of recent lunar craters have been determined in a variety of ways, and some results are conflicting because of the complexity of lunar surface processes. Some samples are related to cratering events in a tenuous manner. Best estimates for the absolute ages of North Ray (Apollo 16), Cone Crater (Apollo 14), and South Ray (Apollo 16) are 50.3 ± 0.8 m.y., 24.4 ± 1.1 m.y., and 2.04 ± 0.08 m.y., respectively (Drozd *et al.*, 1974, and Table II). Rock samples used to obtain ages of North Ray are reliably associated with the crater because the samples came from the rim of the crater and the ages obtained from a number of samples are the same. Krypton exposure ages of North Ray by various workers are consistent with one another (Marti *et al.*, 1973; Drozd *et al.*, 1974), and some fossil particle tracks indicate an age near 50 m.y. (Goswami and Lal, 1974; Crozaz *et al.*, 1974) Microcrater populations indicate an age greater than 14 to 20 m.y. (Morrison *et al.*, 1973). Rock samples used to obtain ages of Cone Crater are also reliably associated with the crater because the samples came from the rim of the crater. Krypton exposure ages of 24.4 m.y. are used, but it should be realized that other methods have yielded a variety of results. The association of rock samples with South Ray is based on the fact that rays from it extend across the Apollo 16 traverse area. A young age for South Ray is supported not only by krypton, neon, and argon exposure ages (Drozd *et al.*, 1974) but also by an anomalously large number of rocks collected during the Apollo 16 mission with microcrater population suggesting an age of 2 to 3 m.y. (Morrison *et al.*, 1973) and fossil particle track ages of 1 to 4 m.y. (Crozaz *et al.*, 1974). Somewhat tenuous geologic arguments indicate ejecta from Tycho disturbed the Apollo 17 surface

TABLE II

Data and procedures used to calibrate Figure 4

	Data derived from crater counts				Assumed cratering size–frequency distribution and calculated limiting diameter				Age of crater	References
Crater and diameter	K	3σ	α	3σ	N_{1_0}	K_a	α_a	D_{CS} (m)	(m.y.)	
Copernicus 9.8×10^4 m					5.9×10^{-4} [1] 8.8×10^{-4}	0.376[1] 0.557	−2.8	58.8[2] ± 17.6	850 ± 0.10	Silver (1971) Soderblom and Lebofsky (1972)
Tycho 8.5×10^4 m	0.191	–	−2.93	–	2.24×10^{-4}	0.141	−2.8	2.1	109 ± 4	Guinness and Arvidson (1977); Shoemaker *et al.*, (1969)
North Ray 980 m	0.118	0.645 0.022	−2.81	± 0.51	1.82×10^{-4}	0.115	−2.8	1.6	50.3 ± 0.8	Drozd *et al.*, (1974)
Cone Crater 390 m	0.055	0.202 0.015	−2.75	± 0.56	0.98×10^{-4}	0.062	−2.8	0.73	24.4 ± 1.1	Drozd *et al.*, (1974)
South Ray 680 m	0.190	–	−4.87	–	0.026×10^{-4}	0.002	−2.8	0.009	2.04 ± 0.08	Drozd *et al.*, (1974)
Hypothetical[3] crater from passive seismometer data	–	–	–	–	0.008×10^{-4} 0.0015×10^{-4}	0.0005 0.0009	−2.8	0.002 0.004	1.0	Duennebier *et al.*, (1975)

[1] N_{1_0} calculated from data of Guinness and Arvidson (1977).

[2] D_{CS} based on unpublished empirical estimate: $D_L = 1.7 D_{CS}$; values of D_{CS} calculated from K_a are 7.0 m and 11.5 m.

[3] Two entries are recorded here because predictions depend on estimated meteoroid impact velocities (see text).

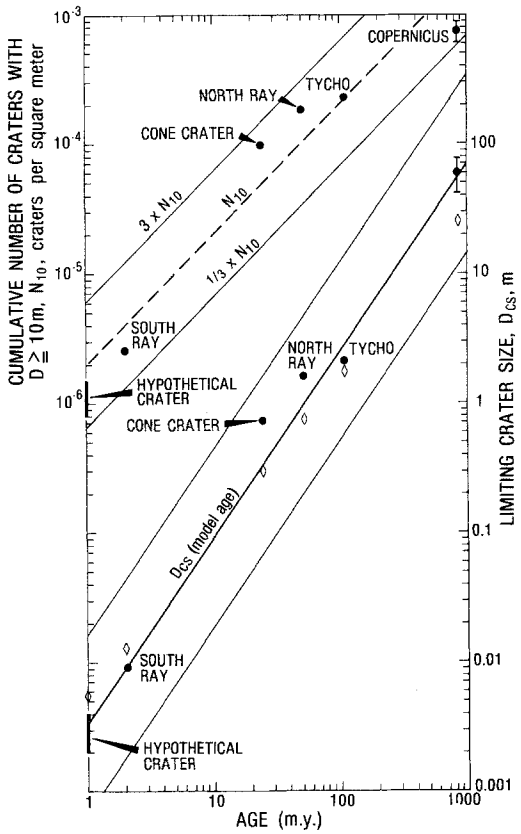

Figure 6. Cumulative number of craters per m^2 with diameters equal to and larger than 10 m and limiting crater size (D_{CS}) as a function of absolute age for Copernicus, Tycho, North Ray, Cone, and South Ray craters. Hypothetical crater calculated using data from the Apollo Passive Seismometer. Heavy dashed line represents cumulative frequencies of craters with diameters of 10 m and larger versus absolute age; because the slope of the line is 1, it represents the expectations for a constant rate of crater production. Heavy solid line is empirical curve of D_{CS} versus age used to assign model ages in Figure 7. Light solid lines indicate best estimate of uncertainties and are 1/3 and 3 times the model age. Dots represent cumulative frequencies of craters with diameters of 10 m and larger (N_{10}) on the ejecta of the indicated crater and the absolute age of the crater (upper part) and limiting crater size (D_{CS}) and absolute age of crater. Diamonds represent values expected for each crater on the basis of mathematical calculations for a constant rate of crater production. Solid bars on left ordinate represent range of values predicted for a 1 m.y.-old crater using data from the Apollo Passive Seismometer (see text).

material 109 m.y. ago (Guinness and Arvidson, 1977), and equally tenuous geologic arguments indicate material 850 m.y. old at the Apollo 12 site originated from Copernicus (Silver, 1971). Despite the geologic uncertainties inherent in associating some samples of known ages with far distant events, these associations are 'best guesses' and they are accepted here. The information used to calibrate Figure 4 is listed in Table II and plotted in Figure 6. The heavy solid line in Figure 6 represents and empirical relation to establish a *model* age using estimated values of D_{CS}.

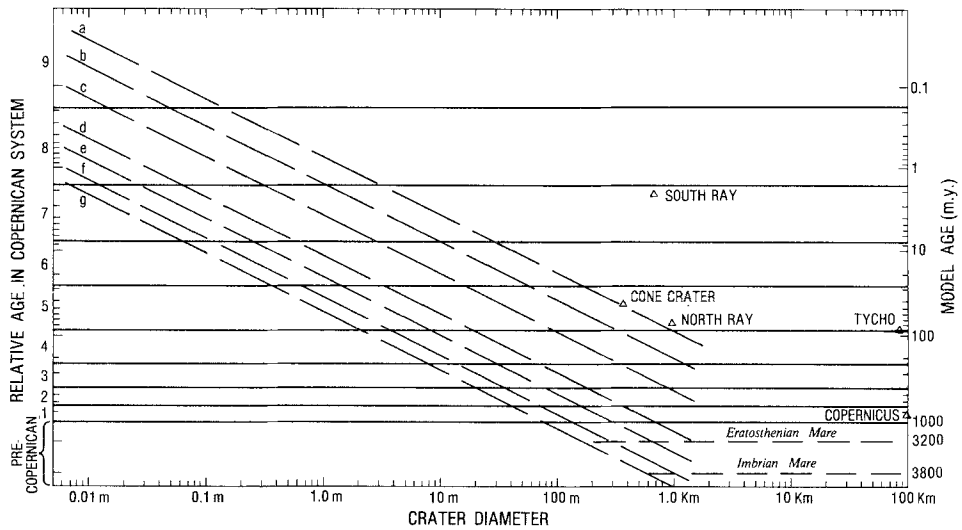

Figure 7. Relations among sizes, morpholgies, relative ages, and model absolute ages of craters from 0.001 m to 100 km. Definitions of morphologic categories appear in Figure 4 and text. Relative ages are indicated on left abscissa and model ages are indicated on right abscissa. Rather broad limits should be placed on the age assigned (1/3 and 3 times the determined value). Procedures outlined in text are invalid for craters and surfaces with model ages above 1000 m.y.

Using the *model* values represented by the solid line in Figure 6, the ordinate of Figure 4 has been assigned model absolute ages in the following way (see Figure 7). The model values for the limiting crater sizes, D_{CS}, corresponding to 1, 10, 100, and 1000 m.y. are about 0.0034, 0.091, 2.5, and 80 m. The intersection of vertical projections of these diameters to the lower diagonal line representing the '*g*' crater morphology group define points, and the horizontal lines through these points correspond to the appropriate isochrons (see Figure 7). Individual craters can be located on the diagram in a similar fashion and their model ages determined. The horizontal position of Copernicus is fixed by the intercept of D_{CS} (58.8 ± 17.6 m) with the lower boundary diagonal of the morphologic types and its diameter (98 km). Thus Copernicus belongs in the relative age group 1. Similarly, Tycho is located at the boundary between relative age groups 4 and 5, and its model age is slightly less than 100 m.y. North Ray is located in the lower part of the age group 5 by virtue of the value of D_{CS} of 1.6, and its horizontal position by virtue of its diameter places it near the boundary between morphologic categories *a* and *b* – a result entirely consistent with descriptions of North Ray (Hodges *et al.*, 1973) and the scarce but observable secondary craters. Model ages do not reveal the actual twofold difference in ages between Tycho and North Ray. For Cone Crater, 390 m across, the limiting crater size, D_{CS}, is 0.73 m so that Cone Crater must be Copernican 5 in age and, like North Ray, close to the boundary between morphologic categories *a* and *b* – again a result consistent with the characteristics of the crater which are very similar to North Ray in morphology (including the presence of secondary impact craters). South Ray becomes Copernican 7 in age with a relatively unmodified morphology.

Calibration of Figure 4 (see Figure 7) is not precise. Model ages of Cone Crater are about 1.8 times larger than the actual age, and the model age of Tycho is only 1.3 times that of North Ray, whereas the correct value is 2.2. Thus, inferred ages should be given rather broad limits – say to a factor of 3 (or 1/3). Such broad limits are corroborated by calculating the cumulative frequencies of craters 25 m across for Tycho (ejecta and playa) and 70 m across for Copernicus (ejecta and floor) from the equations of Guinness and Arvidson (1977) and then computing K_a, D_{CS}, and the cumulative frequency of craters with $D \geqq 10$ m (N_{10}) with the model exponent of (−) 2.8*. In these calculations, ages inferred from the values K_a, N_{10}, and D_{CS} fall within a factor of 1/3 of the actual age with one exception which is 1/4 of the actual age (Copernicus floor). As an example, the data indicate that the model age of Cone Crater is 42 m.y. but the range of model ages would be from 14 m.y. to 126 m.y.

The procedures described above should not be applied to pre-Copernican surfaces (> 1.0 g.y.). Experience suggests that D_L diameters will yield results that are more consistent with the data. For example, the diameter in Figures 4 and 7 corresponding to Imbrian mare is 600 m, but D_L values for Imbrian mare should not exceed the D_L value of 472 m (Boyce *et al.*, 1974). Upper limits for the D_L values for Imbrian are established by those of the Cayley Formation, which are near 560 m; those corresponding to the Imbrian impact event are near 1400 m (Boyce *et al.*, 1974).

6. Present-Day Flux

Present-day fluxes of objects have been estimated with the Apollo Passive Seismometer (Duennebier *et al.*, 1975). The seismometer results are based chiefly on correlations of seismic signals produced by the impacts of various Apollo spacecraft stages with subsequent natural seismic events. Assuming an impact velocity of 22.5 km sec^{-1}, $10^{-7.70}$ impacts/km^2-yr occur for objects with masses of $10^{2.25}$ kg and larger. For a velocity at impact of 14.5 km sec^{-1}, this rate is $10^{-7.22}$ impacts/km^2-yr. Subsequent estimates for mass-frequency distributions of the meteoroid flux depend solely on the crater scaling laws employed and the form of the crater production curve employed in the calculation.

In this paper, the scaling law employed is

$$E = 7.79 \times 10^4 D^{3.6}, \tag{4}$$

where E is the kinetic energy of the impacting object or meteoroid (in joules) and D is the crater diameter (in meters). This scaling law is based on the results of impacts of spacecraft with the Moon (Whitaker, 1972; Table III). This equation predicts crater diameters of 37.2 m and 31.2 m for $10^{2.25}$ kg meteoroids at velocities of 20 km sec^{-1} and 14.5 km sec^{-1}. These diameters are within the range of sizes of craters of interest.

* In these calculations, the cumulative frequency of the smallest size craters in the distributions of Guinness and Arvidson (1977) are calculated and, then, subsequent calculations assume $N = K_a D^{-2.8}$.

TABLE III

Data on impacts of spacecraft with the Moon and calculated scaling laws[1]

Impact Vehicle	Crater diameter D (m)	Kinetic energy E (J)	E/D^3 ($\times 10^5$)	$E/D^{3.4}$ ($\times 10^5$)	$E/D^{3.6}$ ($\times 10^4$)	$E/D^{4.0}$ ($\times 10^4$)
Ranger 7	14.5	1.25×10^9	4.10	1.41	8.24	2.83
Ranger 8	14.5	1.30×10^9	4.26	1.46	8.57	2.94
Ranger 9	15.5	1.32×10^9	3.55	1.18	6.84	2.29
S-IV-B( )	41.0	4.63×10^{10}	6.72	1.52	7.24	1.64
S-IV-B( )	39.5	4.52×10^{10}	7.33	1.68	8.08	1.86
Average factor	–	–	5.19	1.45	7.79	2.31
Standard error	–	–	± 1.71	± 0.18	± 0.72	± 0.57

[1] Note that $E/D^{3.6} = 7.79 \pm 0.72 \times 10^4$ J/m$^{3.6}$ appears to be the best choice scaling because the standard error is only 9 percent of the factor. Percent errors for other factors are larger than 9 percent.

Our best estimates of the form of the crater production size–frequency distribution are obtained from North Ray and Tycho (See Table II). For North Ray,

$$N = 0.115D^{-2.8}; \tag{5}$$

and for Tycho

$$N = 0.141D^{-2.8}. \tag{6}$$

Again, the craters in these distributions are in the range of sizes of interest.

The expected form and magnitude of the meteoroid flux can be obtained from Equations (4), (5) and (6). Equation (4) can be interpreted in terms of crater diameter and meteoroid mass with assumptions for meteoroid velocities. For a meteoroid velocity of 20 km sec^{-1},

$$D = 8.85\ \mathrm{m}^{0.278}, \tag{7}$$

and for 14.5 km sec^{-1},

$$D = 7.69\ \mathrm{m}^{0.278}; \tag{8}$$

substitutions of Equations (7) and (8) in Equations (5) and (6) give the cumulative flux of meteoroids for the period of time North Ray and Tycho have existed. For North Ray,

$$N = 2.57 \times 10^{-4}\ \mathrm{m}^{-0.78}, \tag{9a}$$

$$N = 3.80 \times 10^{-4}\ \mathrm{m}^{-0.78}; \tag{9b}$$

and for Tycho

$$N = 3.15 \times 10^{-4}\ \mathrm{m}^{-0.78}, \tag{10a}$$

$$N = 4.66 \times 10^{-4}\ \mathrm{m}^{-0.78}. \tag{10b}$$

If the age of North Ray is taken as 50.3 m.y., Equations (9a) and (9b) yield an estimate of the present day flux (in m^{-2} yr^{-1}) as

$$N/t = 5.10 \times 10^{-12} m^{-0.78}, \tag{11a}$$

$$N/t = 7.56 \times 10^{-12} m^{-0.78}; \tag{11b}$$

and, if the age of Tycho is taken as 109 m.y., the present-day flux is given by

$$N/t = 2.89 \times 10^{-12} m^{-0.78}, \tag{12a}$$

$$N/t = 4.28 \times 10^{-12} m^{-0.78}. \tag{12b}$$

For $10^{2.25}$ kg meteoroids at velocities of 20 km sec^{-1}, Equations 11a and 12a give: 0.9×10^{-13} and 0.5×10^{-13} impacts/m^2-yr. These numbers agree within a factor of 5 with the higher velocity meteoroid estimate of the passive seismometer of 0.2×10^{-13} impacts/m^2-yr ($10^{-7.7}$ impacts/km^2-yr). For $10^{2.25}$ kg meteoroids at velocities of 14.5 km sec^{-1} Equations (11b) and (12b) give 1.3×10^{-13} and 0.8×10^{-13} impacts/m^2-yr. These numbers agree within a factor of 3 with the lower velocity meteoroid estimate of the passive seismometer of 0.6×10^{-13} impacts/m^2-yr ($10^{-7.22}$ impacts/km^2-yr). Thus, the integrated meteoroid flux appears to have been fairly constant through approximately the last 100 m.y. and possibly 1000 m.y. If there have been any changes at all, the flux appears to have decreased $\simeq$ 1/3 to 1/2, but the rather coarse resolution of the data do not yield sufficiently precise conclusions about changes. The calculations made from the data of Guinness and Arvidson (1977) combined with our data for South Ray and our analysis of the Apollo Passive Seismometer data would imply a constant flux. The Passive seismometer results have been extrapolated to 1 m.y. ago in Figure 6 using the equations developed previously.

Correlation of these results with other results for both smaller and larger craters imply that the form of the distributions of objects striking the Moon varies with size of the object. Microcraters on lunar rocks (Morrison *et al.*, 1973) implies that

$$\phi = 5.5 \times 10^{-9} \text{ m}^{-1.21} \text{ (impacts/m}^2\text{-yr)},$$

where m, the impacting object mass in grams, is in the range of 10^{-8} to 10^{-6}.

Our results imply that

$$\phi = 2.5 \text{ to } 10 \times 10^{-10} m^{-0.78},$$

where m, the impacting object mass in grams, is close to 10^5. These two fluxes intersect at values near 10^1 to 10^3 g. The size–frequency distribution of craters $\simeq$500 m–2 km (Neukum, 1977) implies a third form to the flux of

$$\phi \propto m^{-0.93}.$$

Thus, the form of the mass distribution of objects impacting the Moon varies with the size of the object.

7. Conclusions

(1) There are two types of size-frequency distributions of small lunar craters (1 m to about 100 m across): (1) crater production distributions and (2) steady-state distributions. For the crater production distribution, which is a function of the mass–frequency distribution of impacting objects that produce the craters, the cumulative numbers of small craters is an inverse function of a power of crater diameter that is near 2.8, and such a function implies that the cumulative number of impacting objects is an inverse function of a power of their masses near 0.78.

(2) Each morphologic type of craters larger than about 10 m within the steady-state appears to have size–frequency distributions similar to the steady-state distribution, a result suggesting that each morphologic type is in a steady state. This matter is partly clouded by variations of crater morphologies in layered materials, and data on craters 1 to 10 m across obtained from Ranger 9 pictures indicate that these craters may not behave in the same manner as those greater than 10 m.

(3) Although the rate of impacting objects producing small lunar craters may have declined over the last 1000 m.y., the resolution of the data on crater size-frequency distributions suggests that the rate could have been constant within rather broad limits (within 1/3 and 3 times the calculated rate for Tycho).

(4) The assumed relations among sizes, crater morphologies, and relative ages used in large-scale geologic mapping of Apollo landing sites can be modified to include estimates of absolute ages.

Acknowledgements

This paper was prepared as part of NASA Contract W13, 130. The authors are indebted to N. J. Trask, D. E. Wilhelms, and M. H. Carr for their critical reviews.

References

Boyce, J. M., Dial, A. L., and Soderblom, L. A.: 1974, 'Ages of the lunar nearside light plains and maria', *Proc. 5th Lunar Sci. Conf., Suppl. 5, Geochim. Cosmochim. Acta*, **1**, 11–23.

Chapman, C. R.: 1968, 'Interpretation of diameter-frequency relation for lunar craters photographed by Rangers VII, VIII, and IX', *Icarus* **8**, 1–22.

Crozaz, G., Drozd, R. K., Hohenberg, C. M., Morgan, C. J., Ralston, C. E., Walker, R., and Yuhas, D.: 1974 'Lunar surface dynamics: Some general conclusions and new results from Apollo 16 and 17', *Proc. 5th Lunar Sci. Conf., Suppl. 5, Geochim. Cosmochim. Acta* **3** 2475–2499.

Drozd, R. K., Hohenberg, C. M., Morgan, C. J., and Ralston, C. E.: 1974, 'Cosmic-ray exposure history at the Apollo 16 and other lunar sites: lunar surface dynamics', *Geochim. Cosmochim. Acta* **38**, 1625–1642.

Duennebier, F., Dorman, J., Lammlein, D., Latham, G., and Nakumura, Y.: 1975, 'Meteoroid flux from passive seismic experiment data', *Proc. Sixth Lunar Sci. Conf., Suppl. 6, Geochim. Cosmochim. Acta* **2**, 2417–2426.

Gault, D. E.: 1970, 'Saturation and equilibrium conditions for impact cratering on the lunar surface: criteria and implications', *Radio Science* **5**, 273–291.

Gilbert, G. K.: 1893, 'The Moon's face: a study of the origin of its features', *Philosophical Soc. of Washington, Bull.* **VII** 241–292.

Goswami, J. N. and Lal, D.: 1974, 'Cosmic ray irradiation pattern at the Apollo 17 site: implications to lunar regolith dynamics', *Proc. 5th Lunar Sci. Conf., Suppl. 5, Geochim. Cosmochim. Acta* **3**, 2643–2662.

Guinness, E. A. and Arvidson, R. E.: 1977, 'On the constancy of the lunar cratering flux over the past 3.3×10^9 yr', *Proc. 8th Lunar Sci. Conf. Suppl. 8, Geochim. Cosmochim. Acta* 3475–3494.

Hodges, C. A., Muehlberger, W. R., and Ulrich, G. E.: 1973, 'Geologic settling of Apollo 16', *Proc. 4th Lunar Sci. Conf., Suppl. 4, Geochim. Cosmochim. Acta* **1**, 1025.

Langley Research Center: 1967a, 'Preliminary geologic evaluation and Apollo landing analysis of areas photographed by Lunar Orbiter II', Langley Research Center Working Paper, LWP-363.

Langley Research Center: 1967b, 'Preliminary geologic evaluation and Apollo landing analysis of areas photographed by Lunar Orbiter III', Langley Research Center Working Paper, LWP-407.

Marcus, A. H.: 1970, 'Comparison of equilibrium size distributions for lunar craters', *J. Geophys. Research* **75**, 4977–4984.

Marti, K., Lightner, B. D., and Osborn, T. W.: 1973, Krypton and Xenon in some lunar samples and the age of North Ray crater, *Proc. 4th Lunar Sci. Conf., Suppl. 4, Geochim. Cosmochim. Acta* **2**, 2037–2048.

Moore, H. J.: 1964, 'Density of small craters on the lunar surface', in *Astrogeologic Studies Ann. Prog. Report, Aug. 24, 1962–July 1, 1963, pt. D*, U.S. Geol. Survey open-file report, pp. 34–51.

Moore, H. J.: 1971. 'Geologic interpretation of lunar data', *Earth-Science Review* **7**, 5–33.

Moore, H. J., Lugn, R. V., and Newman, E. B.: 1974, 'Some morphometric properties of experimentally cratered surfaces', *U. S. Geol. Survey Jour. Research* **2**, 279–388.

Morrison, D. A., McKay, D. S., Fruland, R. M., and Moore, H. J.: 1973, 'Microcraters on Apollo 15 and 16 rocks', *Proc. 4th Lunar Sci. Conf., Suppl. 4, Geochim. Cosmochim. Acta* **3** 3235–3253.

National Aeronautics and Space Administration: 1966, 'Ranger IX photographs of the Moon', NASA Spec. Publ. SP-112, 17 pp., 170 plates.

National Aeronautics and Space Administration: 1978, 'Standard techniques for presentation and analysis of crater size–frequency data', NASA Tech. Memo. 79730, 20 pp.

Neukum, Gerhard: 1977, 'Different ages of lunar light plains', *The Moon* **17**, 383–393.

Neukum, G., Konig, B., and Arkani-Hamed, J.: 1975, 'A study of lunar impact crater size-distributions', *The Moon* **12**, 201–229.

Quaide, W. L. and Oberbeck, V. R.: 1968, 'Thickness determinations of the lunar surface layer from lunar impact craters', *Jour. Geophys. Res.* **73**, 5247–5270.

Shoemaker, E. M.: 1965, 'Preliminary analysis of the lunar surface in Mare Cognitum', in *Ranger VII part II, Experimenter's Analyses and Interpretations*, Calif. Inst. Tech., Jet Propulsion Lab. Tech. Rept. 32-700, pp. 75–134.

Shoemaker, E. M., Morris, E. C., Batson, R. M., Holt, H. E., Larson, K. B., Montgomery, D. R., Rennilson, J. J. and Whitaker, E. A.: 1969, 'Television observations from Surveyor', in *Surveyor Program Results*, Natl. Aeronautics and Space Admin. Spec. Publ. NASA SP-184, 19–128.

Silver, L.: 1971, 'U–Th–Pb isotope systems in Apollo 11 and 12 regolithic materials and a possible Copernicus impact event', *EOS, Trans. Amer. Geophys. Union* **52**, p. 534.

Soderblom, L. A.: 1970, 'A model for small-impact erosion applied to the lunar surface', *Jour. Geo-Phys. Research* **75**, 2655–2661.

Soderblom, L. A. and Lebofsky, L. A.: 1972, 'Technique for rapid determination of relative ages of lunar areas from orbital photography', *Jour. Geophys. Research* **77**, 279–296.

Swann, G. A. and Reed, V. S.: 1974, 'A method for estimating the absolute ages of small Copernican craters and its application to the determination of Copernican meteorite flux', *Proc. 5th lunar Sci. Conf., Suppl. 5, Geochim. Cosmochim. Acta* **1**, 151–158.

Trask, N. J.: 1966, 'Size and spatial distribution of craters estimated from the Ranger photographs', In *Ranger VIII and IX, part II, Experimenters' analyses and interpretations*, Calif. Inst. Tech., Jet Propulsion Lab. Tech. Rept. 32-800, pp. 252–264.

Trask, N. J.: 1967, 'Distribution of lunar craters according to morphology from Ranger VIII and IX photographs', *Icarus* **6**, 270–276.

Trask, N. J.: 1971, 'Geologic comparison of mare materials in the lunar equatorial belt, including Apollo 11 and Apollo 12 landing sites', *Geological Survey Research 1971, Chapter D*, U.S. Geol. Survey Prof. Paper 750-D, p. D-138–D-144.

Whitaker, E. A.: 1972, 'Artificial lunar impact craters: four new identifications', *Apollo 16 Prelim. Sci. Rept., Part I*, Natl. Aeron. and Space Adm., NASA SP-315, pp. 29(39)–29(44).

Appendix - Data on areas, crater sizes, and numbers of craters

I. Eumorphic craters in Sinus Medii (II P 8, counted by Newell J. Trask)

Diameter (in m)	11.2	14.0	16.8	19.6	22.4	28.0	33.6	39.2	44.8	50.4	56.0	63.6	Derived equation: $N=3.25\times10^{-3}D^{-2.07\pm0.05}$
Cumulative number (in $10^{-7}/m^2$)	202	149	95	72	46	33	22	17	13	11	8	5	

II. Eumorphic craters in Western Fecunditatis (II P 28, counted by H. J. Moore on Lunar Orbiter II High Resolution frames H33 and H35; Area counted is $3.78\times10^{7}m^2$)

Diameter interval (in m)	4-8	8-16	16-32	32-64	64-128	Derived equation: $N=2.88\times10^{-4}D^{-2.11\pm0.12}$
Number counted in interval	35	95	28	6	1	fit to cumulative frequencies from 32 to 8 m

III. Craters by morphologic categories in Oceanus Procellarum (counted by D. A. Hahn on Lunar Orbiter III High Resolution frame H199; Area counted is $32.5\times10^{6}m^2$ for craters 50 m and larger and $15.4\times10^{6}m$ for craters 25 to 50 m)

Diameter interval (in m)	25-50	50-75	75-100	100-125	125-150	150-175	175-200	200-225	225-250	250+	Equations fit to craters 175 m across and less
A Number of type 1+2+3+4 craters counted in interval	517	170	79	39	27	11	7	5	1	2	Derived equation: $N=7.51\times10^{-2}D^{-2.26}$
B Number of type 1+2+3 craters counted in interval	243	79	37	17	15	7	5	4	1	2	Derived equation: $N=1.37\times10^{-2}D^{-2.00}$
C Number of type 1+2 craters counted in interval	39	16	9	4	5	4	1	3	0	1	Derived equation: $N=5.60\times10^{-4}D^{-1.53}$
D Number of type 1 craters counted in interval	4	1	3	1	1	1					Derived equation: $N=5.48\times10^{-5}D^{-1.42}$

IV. Craters by morphologic categories in Alphonsus (counted by H. J. Moore on Ranger 9 B-87 and $P_3$12; Area counted is $2.46\times10^{6}m^2$; and $4.4\times10^{3}m^2$)

B-87

Diameter interval (in m)	14.1-20	20-28.3	28.3-40	40-56.6	56.6-80	80-113.1	113.1-160	>160	
A Number of type 1+2+3+4 counted in interval	115	123	88	61	12	6	1	6	Derived equation: $N=0.130\ D^{-2.29\pm0.13}$
B Number of type 1+2+3 counted in interval	89	53	35	16	1	2			Derived equation: $N=0.031\ D^{-2.21\pm0.21}$
C Number of type 1+2 counted in interval	58	26	12	10					Derived equation: $N=0.017\ D^{-2.26\pm0.01}$
D Number of type 1 counted in interval	26	12	6	5					Derived equation: $N=0.0065D^{-2.18\pm0.02}$

$P_3$12

Diameter interval (in m)	1.65-2.33	2.33-3.29	3.29-4.66	4.66-6.58	6.58-9.30	9.30-13.2	
A Number of type 1+2+3+4 counted in interval	85	42	16	10	3	3	Derived equation: $N=0.12\ D^{-2.32\pm0.05}$
B Number of type 1+2+3 counted in interval	52	24	8	5	1	1	
C Number of type 1+2 counted in interval	31	15	6	3	1	1	
D Number of type 1 counted in interval	12	7	4	2	1	1	Derived equation: $N=0.017\ D^{-1.92\pm0.03}$

V. North Ray (counted by J. M. Boyce on Apollo 16 Pan 4623; Area counted is $1.25\times10^{-6}m^2$ annulus around crater)

Diameter interval (in m)	12.51-15.29	15.29-18.07	18.07-20.85	20.85-23.63	23.63-26.41	26.41-29.19	29.19-31.97	31.97-34.75	34.75-37.53	37.53-40.31	40.31-43.09	>43.09	Derived equation: $N=0.1175D^{-2.81\pm0.12}$
Number of craters in interval	28	21	18	8	6	7	2	1	0	2	0	4	fit to craters 15.29 m and larger

VI. Cone Crater (counted by Abra Watkins on Lunar Orbiter High Resolution frame H133; Area counted is $0.272\times10^{9}m^2$ annulus around crater)

Diameter interval (in m)	2.38-3.37	3.37-4.76	4.76-6.73	6.73-9.52	9.52-13.46	13.46-19.04	19.04-26.93	Derived equation: $N=5.495\times10^{-2}D^{-2.75\pm0.13}$
Number of craters in interval	295	112	127	36	23	9	4	fit to craters 4.76 m and larger

VII. South Ray (counted by H. J. Moore on Apollo 16 Pan 4618-4623; Area counted is $1.09\times10^{-6}m^2$ on ejecta)

Diameter interval (in m)	8-9	9-10	10-11	11-12	12-13
Number of craters in interval	5	2	0	1	1